J. Fluid Mech. (1985), *vol.* 153, *pp.* 339–360
Printed in Great Britain

Computation of convective laminar flow in rotating cavities

By JOHN W. CHEW
Theoretical Science Group, Rolls-Royce Limited, Derby

(Received 16 December 1983 and in revised form 10 October 1984)

Numerical predictions are presented for the centrifugally driven free convection in a sealed rotating cavity and for the buoyancy-affected flow through a cavity with an inner cylindrical source and an outer cylindrical sink. Results for a sealed cavity filled with a high-viscosity silicone oil are in good agreement with previously published experimental measurements of the mean Nusselt number. When the heat transfer is conduction-dominated the results away from the cylindrical surface agree with Dorfman's (1968) similarity solution, but as convection becomes important they depart from this solution. In an air-filled cavity, for both the free convection and radial outflow cases, the results away from the cylindrical surface are generally in reasonable agreement with Chew's (1982) similarity solution, although property variations and radial heat conduction do cause some departure from this solution. The extent of the region in which the heat transfer was influenced by the presence of the cylindrical surface, and the Nusselt number distribution in this region are shown to be sensitive to the thermal boundary conditions imposed on this surface.

1. Introduction

In two earlier papers (Chew 1984; Chew, Owen & Pincombe 1984) a finite-difference program for prediction of steady source–sink flow in a rotating cylindrical cavity was described and results for a cavity having a net radial outflow of fluid were presented. This program has now been extended to solve the energy equation in addition to the mass and momentum conservation equations, and to allow for property variations of the fluid. In the present paper numerical results are given for flows which are induced or strongly affected by buoyancy in the centrifugal force field. Three classes of flow are considered: 'free convection' in a sealed cavity filled with a high-viscosity silicone oil; free convection in an air-filled cavity; and the flow in a cavity having a radial outflow of air. Motivation for this work comes from the gas-turbine industry where an understanding of the flow between co-rotating disks is important for estimating disk cooling rates.

Insight into the flow in a finite cavity can be gained from the closely related, but somewhat simpler, case of the flow between two infinite co-rotating disks at different uniform temperatures. Similarity solutions for centrifugally driven flow have been given by several workers. Dorfman's (1968) solution, which assumes a linear temperature profile across the cavity in the solution for the flow field, is valid both for the Ekman-layer regime where separate boundary layers on each disk are separated by a central core and in a merged boundary-layer regime in which there is no central core. Barcilon & Pedlosky (1967) and Hudson (1968) have derived solutions for Ekman-layer flow assuming the temperature in each Ekman layer is equal to that on the adjacent disk. These solutions are valid for air in convection-

dominated conditions at high rotational speed but, owing to the large value of the Prandtl number for the high-viscosity oil, do not apply for this fluid. Further descriptions of these solutions and extensions to include the effects of a radial throughflow of fluid and non-uniform disk temperatures have been given by Chew (1982).

Relevance of the similarity solutions to the flow in a finite cavity is investigated in the present paper. This has previously been discussed, for the sealed cavity, by Barcilon & Pedlosky (1967) and Homsy & Hudson (1969). Barcilon & Pedlosky found that with an insulating cylindrical boundary it was not possible to match their similarity solution to the boundary layer on the cylindrical surface and concluded that it was not the limiting solution of a physically realizable experiment in a closed container. However, Homsy & Hudson showed that if the cylindrical wall was assumed perfectly conducting their zero-order solution for the flow did approach the infinite-disk solution towards the centre of the cavity. Several other workers have used, and further developed, the methods of Barcilon & Pedlosky and Homsy & Hudson to study thermally driven flow in a gas centrifuge (e.g. Matsuda & Hashimoto 1976; Conlisk, Foster & Walker 1982). This approach is superior to the infinite-disk solutions in that account is taken of the cylindrical boundary, but the analysis involved is considerably more complicated and in certain parameter ranges recourse to numerical methods has to be made.

Experimental heat-transfer measurements in a closed cylinder with the disks of uniform temperatures T_0 and T_s have been given by Hudson, Tang & Abell (1978). Axial gap to radius ratios (G) of 0.07 and 0.14 were used and the cavity was filled with silicone oil. Two Nusselt number correlations were obtained, corresponding to two different oils. For a high-viscosity oil (kinematic viscosity $\nu = 3.5 \times 10^{-4}$ m^2/s, Prandtl number $Pr = 3118$) the results were represented by

$$\overline{Nu} = 1.13\, Gr^{0.267} G^{0.054}. \tag{1.1}$$

Here $\overline{Nu}$ is a mean Nusselt number defined by $\overline{Nu} = s\bar{q}/k\,\overline{\Delta T}$, where s is the axial gap between the disks, $\bar{q}$ is the heat flux averaged over the disk area, k is the thermal conductivity and $\overline{\Delta T} = \overline{T}_s - \overline{T}_0$ is the mean temperature difference between the two disks. Gr is a Grashof number defined by $Gr = \Omega^2 b s^3 \beta\, \Delta T/\nu^2$, where Ω is the rotational speed, b is the cavity radius, and β is the coefficient of thermal expansion. The results for a low-viscosity oil, which show similar trends to the laminar Ekman-layer theory, were correlated by

$$\overline{Nu} = 0.533(\beta \overline{\Delta T})^{0.822} Re_\theta^{0.499} G^{0.825} \tag{1.2}$$

where Re_θ ($= \Omega b^2/\nu$) is a rotational Reynolds number.

Following a brief description of the mathematical model in the next section, numerical results will be presented for the cavity filled with a high-viscosity oil, as studied by Hudson *et al.*, in §3, and for an air-filled sealed cavity in §4. Computations were also attempted for Hudson *et al.*'s low-viscosity-oil case. However, owing to difficulties encountered in obtaining convergence of the iterative solution, results were only obtained for conduction-dominated conditions, and their inclusion, other than for demonstrating the accuracy of the solution method, was not considered worth while. For the air-filled cavity particular attention has been given to the effect of applying different temperature distributions on the disks and the influence of the thermal boundary condition on the enclosing cylindrical surface. In §5 results are given for the case of radial outflow influenced by buoyancy. The main conclusions are then summarized in §6.

2. The mathematical model

2.1. *The governing equations*

The following form of the axisymmetric momentum, mass and energy conservation equations was used:

$$\frac{1}{r}\frac{\partial}{\partial r}(\rho r u^2)+\frac{\partial}{\partial z}(\rho u w) = -\frac{\partial p}{\partial r}+\frac{\rho v_\phi^2}{r}+\frac{1}{r}\frac{\partial}{\partial r}\left(\mu r\frac{\partial u}{\partial r}\right)+\frac{\partial}{\partial z}\left(\mu\frac{\partial u}{\partial z}\right)+\frac{1}{3r}\frac{\partial}{\partial r}\left(\mu r\frac{\partial u}{\partial r}\right)$$
$$-\frac{2}{3}\frac{u}{r}\frac{\partial \mu}{\partial r}-\frac{4}{3}\frac{\mu u}{r^2}-\frac{2}{3}\frac{\partial}{\partial r}\left(\mu\frac{\partial w}{\partial z}\right)+\frac{\partial}{\partial z}\left(\mu\frac{\partial w}{\partial r}\right), \tag{2.1}$$

$$\frac{1}{r}\frac{\partial}{\partial r}(\rho r u v_\phi)+\frac{\partial}{\partial z}(\rho v_\phi w) = -\frac{\rho u v_\phi}{r}+\frac{1}{r}\frac{\partial}{\partial r}\left(\mu r\frac{\partial v_\phi}{\partial r}\right)+\frac{\partial}{\partial z}\left(\mu\frac{\partial v_\phi}{\partial z}\right)-\frac{v_\phi}{r}\frac{\partial \mu}{\partial r}-\mu\frac{v_\phi}{r^2}, \tag{2.2}$$

$$\frac{1}{r}\frac{\partial}{\partial r}(\rho r u w)+\frac{\partial}{\partial z}(\rho w^2) = -\frac{\partial p}{\partial z}+\frac{1}{r}\frac{\partial}{\partial r}\left(\mu r\frac{\partial w}{\partial r}\right)+\frac{\partial}{\partial z}\left(\mu\frac{\partial w}{\partial z}\right)$$
$$+\frac{1}{3}\frac{\partial}{\partial z}\left(\mu\frac{\partial w}{\partial z}\right)-\frac{2}{3}\frac{\partial}{\partial z}\left(\frac{1}{r}\frac{\partial (ru)}{\partial r}\right)+\frac{1}{r}\frac{\partial}{\partial r}\left(\mu r\frac{\partial u}{\partial z}\right), \tag{2.3}$$

$$\frac{1}{r}\frac{\partial}{\partial r}(\rho r u)+\frac{\partial}{\partial z}(\rho w) = 0, \tag{2.4}$$

$$\frac{1}{r}\frac{\partial}{\partial r}(\rho r u h)+\frac{\partial}{\partial z}(\rho w h) = \frac{1}{r}\frac{\partial}{\partial r}\left(\frac{rk}{C_p}\frac{\partial h}{\partial r}\right)+\frac{\partial}{\partial z}\left(\frac{k}{C_p}\frac{\partial h}{\partial z}\right)+\frac{1}{r}\frac{\partial}{\partial r}\left[\left(\mu-\frac{k}{C_p}\right)r\frac{\partial}{\partial r}\left(\frac{u^2+v_\phi^2+w^2}{2}\right)\right]$$
$$+\frac{\partial}{\partial z}\left[\left(\mu-\frac{k}{C_p}\right)\frac{\partial}{\partial z}\left(\frac{u^2+v_\phi^2+w^2}{2}\right)\right]$$
$$+\frac{1}{r}\frac{\partial}{\partial r}\left[r\mu\left(\frac{u}{3}\frac{\partial u}{\partial r}-\frac{2}{3}\frac{u^2}{r}-\tfrac{2}{3}u\frac{\partial w}{\partial z}-\frac{v_\phi^2}{r}+w\frac{\partial u}{\partial z}\right)\right]$$
$$+\frac{\partial}{\partial z}\left[\mu\left(u\frac{\partial w}{\partial r}+\frac{w}{3}\frac{\partial w}{\partial z}-\frac{2}{3}\frac{w}{r}\frac{\partial (ru)}{\partial r}\right)\right], \tag{2.5}$$

where h is the stagnation enthalpy defined by

$$h = C_p T+\tfrac{1}{2}(u^2+v_\phi^2+w^2). \tag{2.6}$$

Here u, v_ϕ and w are the radial, tangential and axial components of velocity in the stationary cylindrical coordinate system (r, ϕ, z). T, μ, k and C_p denote temperature, dynamic viscosity, thermal conductivity and specific heat at constant pressure respectively. C_p has been assumed to be constant.

For the sealed cavities the boundary conditions for the velocity were given by the no-slip condition on the surfaces, $z = 0$, $z = s$ and $r = b$, and by symmetry at the axis of rotation, $r = 0$. Several different temperature boundary conditions were investigated. These are described in the following sections. The modifications to these conditions for source–sink flow are given in §5.

2.2. *The finite-difference solution*

Finite-difference solutions of the above equations were obtained using the techniques described by Chew (1984). The computer program employed was a modified version of the TEACH program of Gosman & Ideriah (1976). In this approach a staggered grid is defined, with v_ϕ and p being calculated at the main grid points and u and w being

calculated at radially and axially staggered locations which are midway between the main grid points. Finite-difference representations of (2.1)–(2.5) are derived from a control-volume approach and are then solved iteratively using the 'SIMPLE' algorithm defined by Patankar & Spalding (1972). Modifications to the standard method included the introduction of step changes on grid size to give sufficient resolution in the boundary layers and a more accurate solution of the pressure correction equations at each iteration than had previously been used. This latter modification was found to improve the convergence of the iterative solution. The 'hybrid' differencing method employed gives a first-order truncation error when upwind differencing is used for the advective terms. For cell Reynolds numbers less than 2, central differencing is used for these terms and the scheme is then second-order accurate.

It was straightforward to modify the iterative solution scheme used in the earlier studies of incompressible flow to include solution of the energy equation and to allow variable properties. After each update of the velocity and pressure fields, an 'improved' solution for the temperature is calculated from the energy equation. The fluid properties corresponding to the new temperature field are then used in the next iteration for the velocities. The practice of solving equations for the pressure corrections to a given accuracy, while calculating the solutions of the other equations from a single double sweep of the 'line-by-line' procedure, was again found to be effective in improving the rate of convergence. As for the other variables, under-relaxation was used for the temperature solution and the rate of convergence of the iterative method depended strongly on the choice of this factor.

The computing time required to obtain a solution varied considerably for different cases. In general, the time required increased with the rotational Reynolds number and the number of points in the finite-difference grid and was sensitive to the choice of under-relaxation factors. Typically about 30 min of c.p.u. time on the CDC7600 computer was used to obtain convergence for one particular case.

In order to produce streamline plots, values for the stream function were calculated from the results for the velocities. The method used was similar to that for incompressible flow with the stream function (ψ) being defined, so that

$$\frac{\rho u}{\rho_{\text{ref}}} = -\frac{1}{r}\frac{\partial \psi}{\partial z}; \quad \frac{\rho w}{\rho_{\text{ref}}} = \frac{1}{r}\frac{\partial \psi}{\partial r}, \tag{2.7}$$

where the subscript ref denotes reference conditions. Contour plots of ψ and T were produced using a standard graphics package. As this required interpolation of the results on to a coarser grid than that used for the finite-difference calculation, some loss of accuracy in this process must be expected. Thus, although this representation of the results does give a valuable insight into the solutions, the finer detail in those plots should be regarded with some caution.

2.3. *Accuracy of the numerical solutions*

Results for a cavity filled with low-viscosity oil with isothermal disks, as studied experimentally by Hudson *et al.* (1978), provide a good example of the agreement between numerical and analytical results. In this example all fluid properties, apart from density and the coefficient of thermal expansion, were assumed constant. At high Reynolds number thin boundary layers develop and for sufficiently small $|\beta \Delta T|$ the similarity solution for the velocities and temperature is expected to be almost exact away from the cylindrical surface. With an adiabatic condition at the cylindrical surface numerical results were obtained for $Re_\theta = 3.15 \times 10^5$,

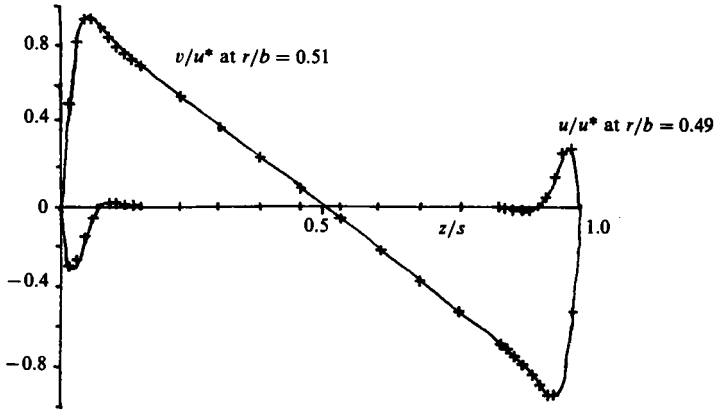

FIGURE 1. Radial and tangential velocities for thermally-driven flow of a low-viscosity oil: +, numerical; ——, similarity solution.

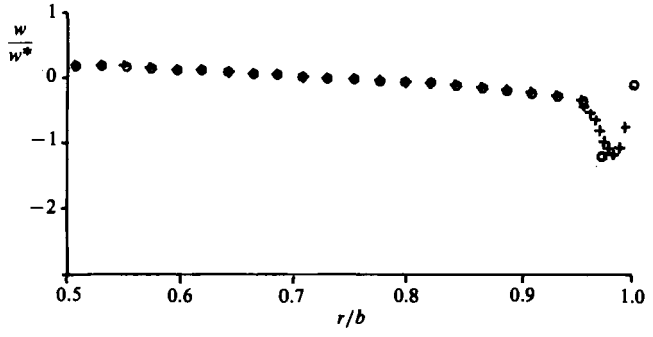

FIGURE 2. Axial velocity at $z/s = 0.5$ for thermally driven flow of a high-viscosity oil, $Re_\theta = 5000$, $\beta\Delta T = -0.0192$: ○, +, numerical results from different finite-difference grids.

$\beta\Delta T = -0.00134$, $Pr = 7.19$ and $G = 0.07$. As can be seen from the radial and tangential velocity distributions near mid-radius, shown in figure 1, excellent agreement was found between numerical and analytical results. Note that the tangential velocity here is referred to a rotating frame so that $v = v_\phi - \Omega r$ and the velocities in this figure are normalized with the factor

$$u^* = \tfrac{1}{4}\beta|\Delta T|\,\Omega r. \tag{2.8}$$

Further comparisons with analytical and experimental results are given in the following sections and in the earlier incompressible flow studies by Chew (1984) and Chew *et al.* (1984).

An example of the use of a step change in grid size to obtain resolution in the boundary layers is shown in figure 2. Here, numerical predictions of the axial velocity at the mid-axial position on two different finite-difference grids are shown for the flow of a high-viscosity oil in a sealed cavity with $Re_\theta = 5\times10^3$, $\beta\Delta T = -0.0192$, $Pr = 3118$ and $G = 0.07$. The non-dimensionalizing factor in this case is

$$w^* = \frac{\beta|\Delta T|\,\Omega b}{4Re_\theta^{\frac{1}{2}}}. \tag{2.9}$$

	High-viscosity oil	Air
ρ (kg/m^3)	$970[1-\beta(T-T_{ref})]$ ($\beta = 0.00096$ K^{-1})	p/RT† ($R = 287.2$ J kg^{-1} K^{-1})
μ (kg/ms)	0.3395	$1.46\times10^{-6}\,T^{\frac{3}{2}}/(110+T)$†
k (W/mK)	0.159	$0.0242+7.91\times10^{-5}(T-273)-3.29\times10^{-8}(T-273)^2$†
C_p (J/kg K)	1461	1012
Pr at reference conditions	3118	0.72

† Temperature in kelvin.

Table 1. Properties of the two fluids considered

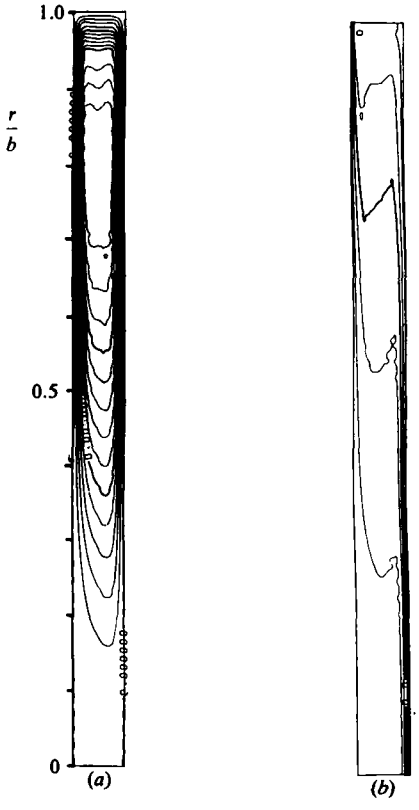

FIGURE 3. Thermally driven flow of a high-viscosity oil, $Re_\theta = 5000$, $\beta\Delta T = -0.0192$; (*a*) streamlines at intervals of 3×10^{-9} m^3/s, (*b*) isotherms at $0.2\Delta T$ intervals.

Considering that, for the coarser grid, only one radial grid line lies within the boundary layer on the surface at $r = b$, it is perhaps surprising that the two sets of results are so close. Outside the boundary layer the results agree almost exactly, while the higher gradients within the boundary layer lead to some difference between the two finite-difference solutions.

Although, as in the above example, some of the results presented here have been repeated using different grid sizes to ensure that truncation error was not significant, this has not been done in every case. However, care was taken to ensure that

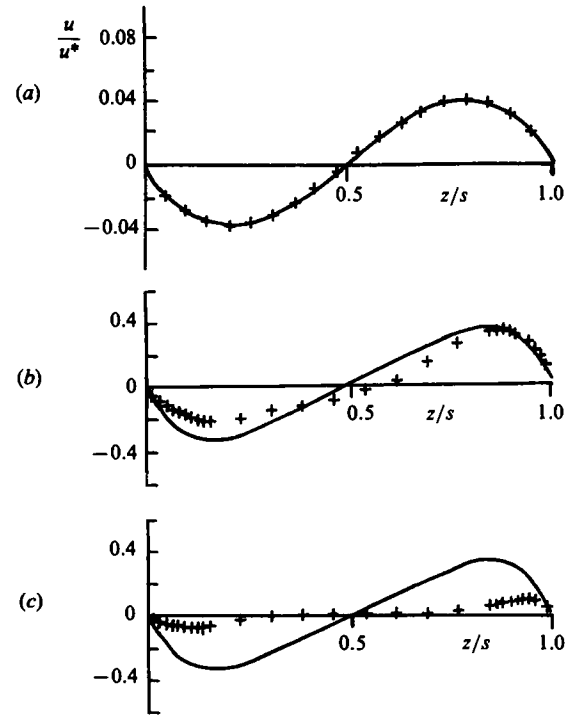

FIGURE 4. Radial velocity at $r/b = 0.49$ for thermally driven flow of a high-viscosity oil: +, numerical results; ——, Dorfman (1968). (*a*) $Re_\theta = 250$, $\beta\Delta T = -0.00096$. (*b*) $Re_\theta = 5000$, $\beta\Delta T = -0.00192$. (*c*) $Re_\theta = 5000$, $\beta\Delta T = -0.048$.

reasonable grid definition was attained in the boundary layers. Typically, five or more grid points are located in the boundary layers. This compares favourably with other workers' practice; for example, in his study of the transient, thermally driven flow in a rotating annulus, Williams (1967) required that at least three points should be located within each layer.

3. An oil-filled sealed cavity

The problem considered in this section is of a sealed cavity filled with a high-viscosity silicone oil, as studied experimentally by Hudson *et al.* (1978). In addition to providing a good test for the numerical method this also leads to a better understanding of the experimental work, as the numerical solutions give the temperature and velocity fields throughout the cavity, whereas only mean heat-transfer rates have been measured experimentally.

To simulate Hudson *et al.*'s experimental conditions, the two disks were supposed to have uniform temperatures T_0 and T_s, and the cylindrical surface was assumed adiabatic in the numerical calculations. The radius of the cavity was also chosen to model the experimental apparatus so that $b = 139.8$ mm and the spacing between the disks s was taken as 9.7 mm, which was the smallest gap for which measurements were made. The properties of the oil (and of air) are given in table 1. Note that, owing to the high Prandtl number of the oil, the similarity solutions given by Barcilon and Pedlosky (1967), Hudson (1968) and Chew (1982), which assume the Ekman-layer

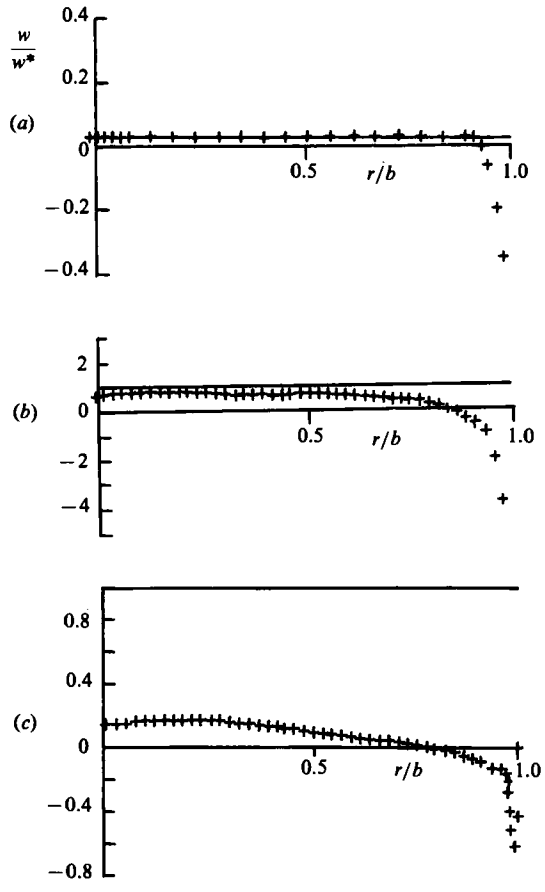

FIGURE 5. Axial velocity at $z/s = 0.5$ for thermally driven flow of a high-viscosity oil: +, numerical results; ——, Dorfman (1968). (*a*) $Re_\theta = 250$, $\beta\Delta T = -0.00096$. (*b*) $Re_\theta = 5000$, $\beta\Delta T = -0.00192$. (*c*) $Re_\theta = 5000$, $\beta\Delta T = -0.048$.

thickness to be much less than the thermal boundary-layer thickness, are invalid in this case. However, Dorfman's (1968) solution may still be applied for this fluid.

The highest rotational speed considered for this case corresponds to $Re_\theta = 5000$. Streamline and isotherm plots for this speed with $\beta\Delta T = -0.0192$ are shown in figure 3. It is apparent that convective effects are important for those conditions. Fluid flows radially inwards next to the hotter, left-hand disk and radially outwards next to the colder, right-hand disk. Where fluid moves axially across the cavity a thermal boundary layer forms on the downstream surface. Owing to the high Prandtl number, the thickness on the thermal layers is less than that of the velocity boundary layers.

Comparisons between Dorfman's similarity solution and the numerical results are shown in figures 4 and 5. In figure 4 the axial variation of the radial velocity near the mid-radial position is shown for three different cases. For $Re_\theta = 250$, $\beta\Delta T = -0.00096$ conduction dominates the heat transfer and, as expected, the numerical and analytical results agree closely. At higher values of Re_θ and $|\beta\Delta T|$ the numerical results depart from Dorfman's solution and are no longer antisymmetric about $z/s = 0.5$ as is predicted for the conduction-dominated flows. The axial velocity

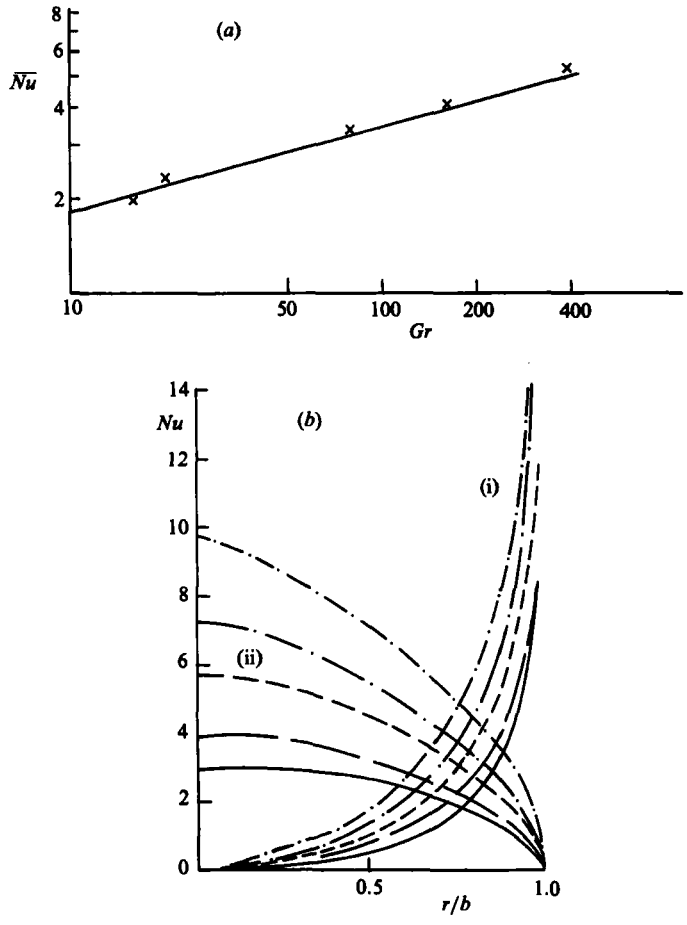

FIGURE 6. Nusselt numbers for the high-viscosity oil. (*a*) Variation of mean Nusselt number with Grashof number: ×, numerical results; ——, equation (1.1). (*b*) Variation of Nusselt number with radius: (i) hot disk (ii) cold disk.

$Re_\theta/10^3$	5	2.5	5	5	5
$-\beta\Delta T$	0.0019	0.0096	0.0096	0.0192	0.048
Numerical results	——	— —	– – –	.—.	.–.–.

at the mid-axial position shown in figure 5 indicates the extent to which the rechannelling of fluid at the cylindrical boundary affects the flow in these three examples. For $Re_\theta = 250$, $\beta\Delta T = -0.00096$ this influence appears to be confined to the region $0.9 < r/b < 1$, while for $Re = 5000$, $\beta\Delta T = -0.048$ the flow throughout the cavity is affected by the rechannelling. At the intermediate conditions $Re_\theta = 5000$, $\beta\Delta T = -0.0019$ the axial velocity does appear to reach an asymptotic value at small radii which is significantly lower than the analytic solution.

Mean and local Nusselt numbers for all the convection-dominated cases that have been studied are shown in figure 6. From figure 6(*a*), which shows the variation of the mean Nusselt number with the Grashof number, the numerical results can be seen to be in good agreement with the experimental correlation equation (1.1). Some differences between the results are to be expected as gravitational effects have not been included here. As expected, the local Nusselt number distribution is very

Case	$Re/10^4$	$\Delta T/T_{max}$	Thermal boundary conditions at $r = b$	Numerical results $\overline{Nu_0}$	Numerical results $\overline{Nu_s}$	Similarity solution $\overline{Nu_0}$	Similarity solution $\overline{Nu_s}$
(i)	1	0.228	$\partial T/\partial r = 0$	1.4	1.4	1.6	0.8
(ii)	2	0.228	$\partial T/\partial r = 0$	1.7	1.7	2.0	0.5
(iii)	2	0.228	$T = T_0 + (z/s)\Delta T$	2.0	0.9	2.0	0.5
(iv)	2	0.391	$T = T_0 + (z/s)\Delta T$	3.0	1.3	2.9	0.3
(v)	2	$0.228(r/b)^2$	$\partial T/\partial r = 0$	1.6	1.6	2.4	−0.9
(vi)	2	$0.391[1-(r/b)^2]$	$\partial T/\partial r = 0$	1.9	1.9	1.6	2.1

TABLE 2. Conditions studied and mean Nusselt numbers for the air-filled sealed cavity

different for the two disks. Heat transfer from the hot disk is greatest at large radii while the heat transfer to the cold disk is greatest at the centre of the disk and falls to zero at $r = b$.

It is interesting to note that in all these cases the Nusselt numbers for the two disks are equal for a value of r/b in the range 0.75–0.8. From streamline plots (e.g. figure 3) and axial velocity profiles (e.g. figure 5) it was observed that a stagnation point in the flow occurs at about this radius.

4. An air-filled sealed cavity

The results given in this section are for a cavity with a radius b of 190 mm and an axial gap s of 50.7 mm. These correspond to the dimensions used in the isothermal flow studies. The properties of air were calculated from the relations given in table 1, with the pressure at the centre of the cavity set equal to 10^5 Pa. Although the perfect-gas law was used to calculate the density, the pressure differences within the cavity are relatively small for the conditions considered here, and so, in effect, density is a function of temperature only.

The different cases studied in this section are summarized in table 2. Note that the parameter $\Delta T/T_{max}$, where T_{max} is the maximum temperature in the cavity is comparable to $\beta \Delta T$ used in the previous section. Several different thermal-boundary conditions have been considered. The cylindrical surface was assumed adiabatic in cases (i), (ii), (v) and (vi), while in the remaining two cases, (iii) and (iv), a linear temperature variation between the values for the two disks was specified on this surface. In all cases the left-hand disk at $z = 0$ is assumed isothermal at the reference temperature of 288 K. The right-hand disk at $z = s$, which is the hotter of the two disks, is also assumed isothermal in cases (i)–(iv), but in (v) and (vi) quadratic temperature variations were used on this disk.

Streamline and isotherm plots for cases (i) and (vi) are given in figure 7. The streamlines for case (i) are typical of conditions (i) to (v), showing Ekman layers on each disk, a boundary layer on the outer cylinder and, away from the outer layer, axial flow from the hot to the cold disk. The flow structure in case (vi), for which the temperature difference across the cavity decreases quadratically from 185 K at $r = 0$, to 0 *at* $r = b$, differs from the other cases in that there is very little rechannelling of fluid at the outer radius and the 'axial wind' flows from the cold disk to the hot disk in the outer part of the cavity. These effects are consistent with the similarity solution (Chew 1982), which predicts a reversal of the axial wind at $r/b = 0.71$ and

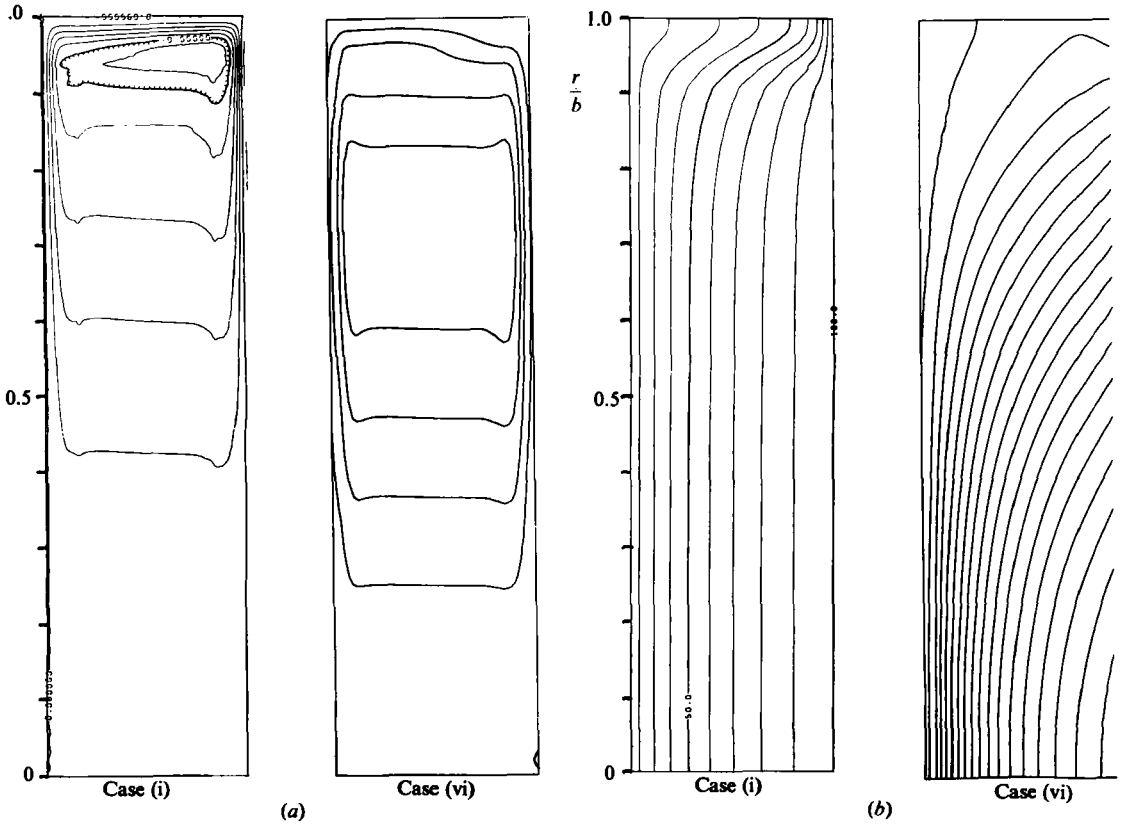

FIGURE 7. Thermally driven flow of air for conditions (i) and (vi) of table 2. (*a*) Streamlines at intervals of 1.5×10^{-6} m^3/s. (*b*) Isotherms at intervals of 10 K.

zero flow in the Ekman layers at $r/b = 1$. The isotherm plots show that the temperature distribution is affected by convection for these conditions. The axial flow across the cavity compresses the isotherms towards the downstream disk while the rechannelling of fluid in the outer layer causes high heat transfer from the hot disk in that region.

Comparisons of non-dimensional axial velocity at $z/s = 0.48$ and radial velocity, tangential velocity and temperature near $r/b = 0.5$, to the similarity solutions are shown in figure 8 for the case (iv). Note that the non-dimensional velocities contain the multiplying factor ρ/ρ_{ref}. This was found to bring the results closer to the similarity solution in which the density is assumed equal to ρ_{ref} in all but the centrifugal force terms. The factor $1/T_{\text{max}}$ was used for the coefficient of thermal expansion β appearing in the similarity solution and in the definition of w^* and u^*. From graph 8(*a*) it appears that recirculation at the edge of the outer layer occurs for these conditions. A similar effect was noted in the isothermal results for source–sink flow at the higher flow rates studied and a recirculating region in the outer layer was predicted in Homsy & Hudson's analytical solutions. The radial velocity profile in figure 8(*b*) shows that the results in the Ekman layer next to the cold disk are in excellent agreement with the theory. In the layer next to the hot disk there are some differences between the numerical and analytical results but, owing to the property variations of the air, these are to be expected. Property variations may also account

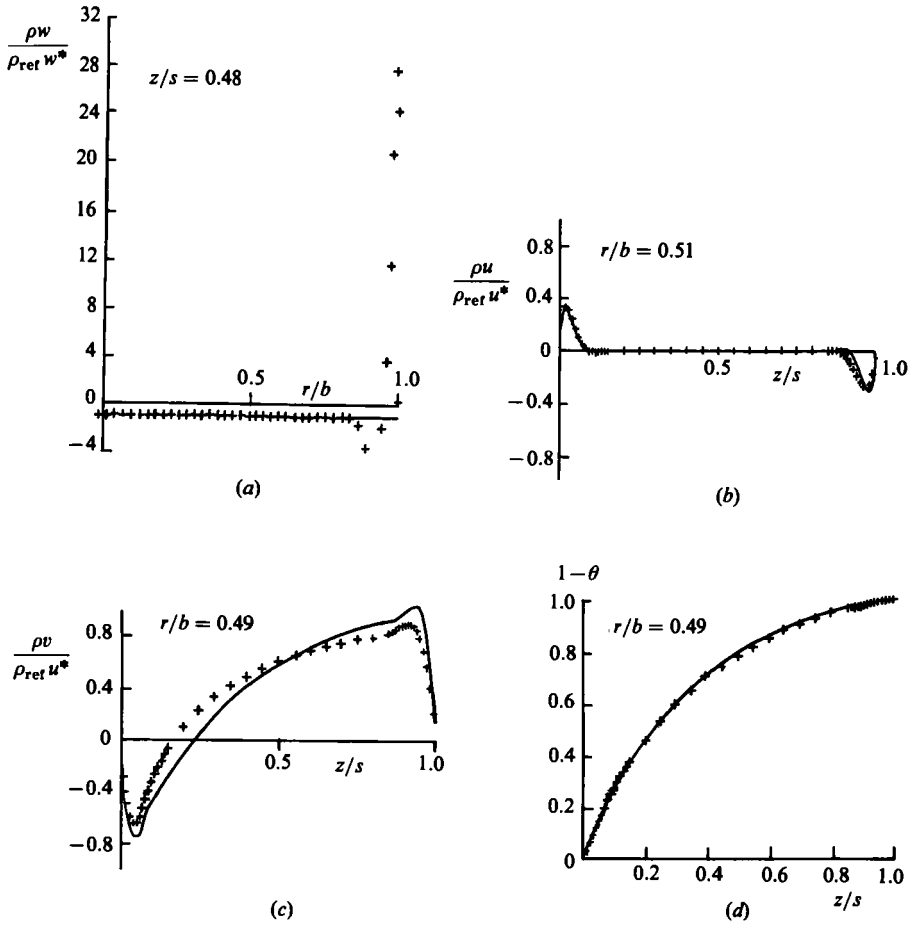

FIGURE 8. Velocity and temperature profiles for thermally driven flow of air: case (iv), $Re_\theta = 2 \times 10^4$, $\Delta T/T_{\max} = 0.391$; +, numerical results; ——, similarity solution.

for the departure of the numerical results for the tangential velocity from the analytical solution, which is apparent from figure 8(*c*). Despite these differences between the two sets of results for the velocities, the temperature profile across the cavity, shown in figure 8(*d*), agrees closely with the similarity solution.

Figure 9 shows the profiles of temperature and of radial and tangential velocity near the mid-radial position for the two examples with non-uniform disk temperatures (cases (v) and (vi)). The non-dimensional temperature is defined, such that $\theta = (T_s - T)/\Delta T$. For case (vi) both the temperature and velocities are in reasonable agreement with the similarity solution. For case (v) the tangential velocity and the temperature show a significant departure from the analytical solution, although the radial velocity is somewhat closer to the similarity solution. The discrepancy is attributed to radial viscous and heat-conduction effects which are neglected in the analytical solution. For a quadratic temperature distribution, the neglect of radial viscous effects in the similarity solution is valid provided the group $|Re_\theta^{\frac{1}{2}}(r^2/bs)\frac{1}{8}\beta\Delta T| \gg 1$. At $r/b = 0.5$ the parameter takes the values 0.9 and 4.8 for

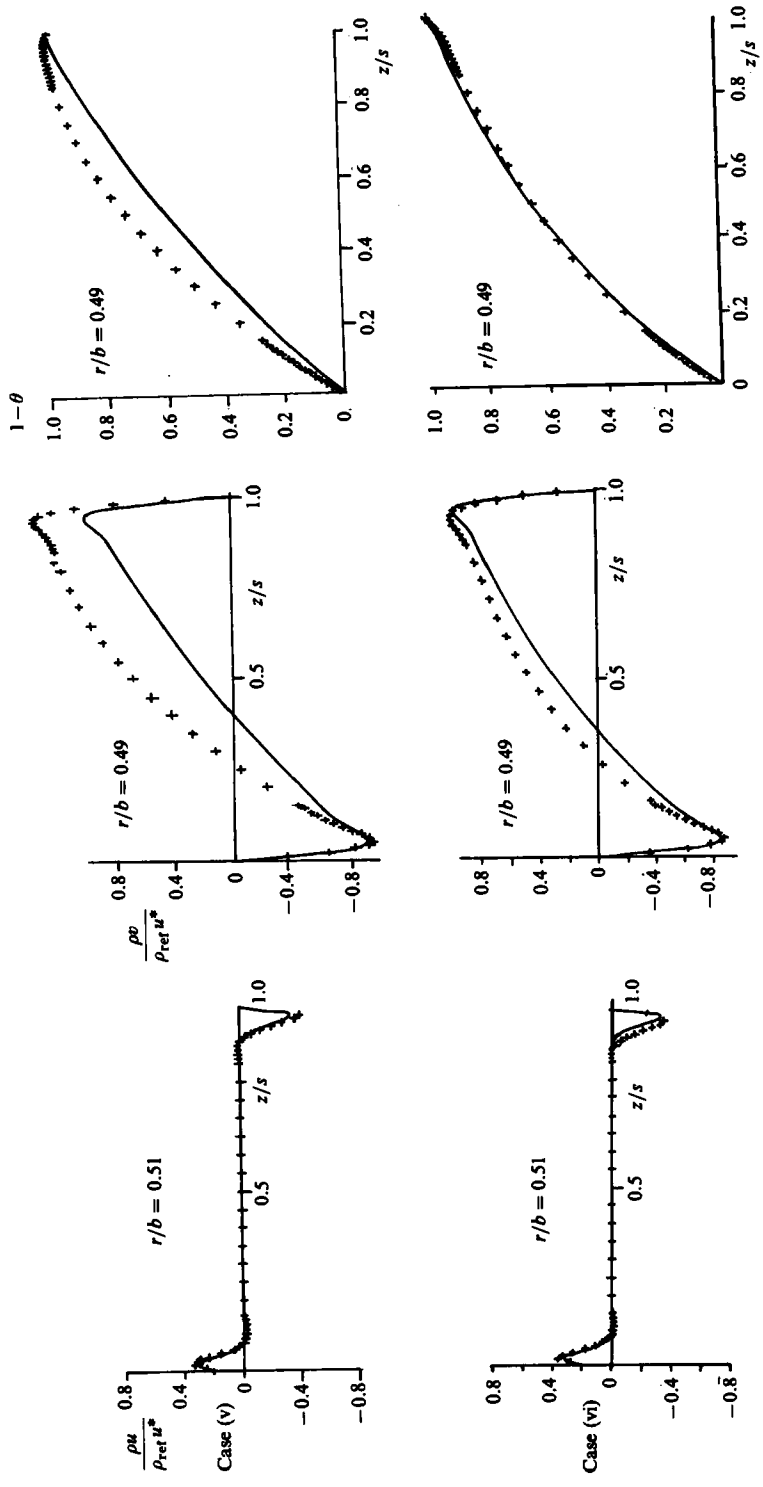

FIGURE 9. Velocity and temperature profiles for thermally driven flow of air: case (v), $Re_\theta = 2 \times 10^4$, $\Delta T/T_{max} = 0.228(r/b)^2$; case (vi), $Re_\theta = 2 \times 10^4$, $\Delta T/T_{max} = 0.391[1-(r/b)^2]$; +, numerical results; ——, similarity solution.

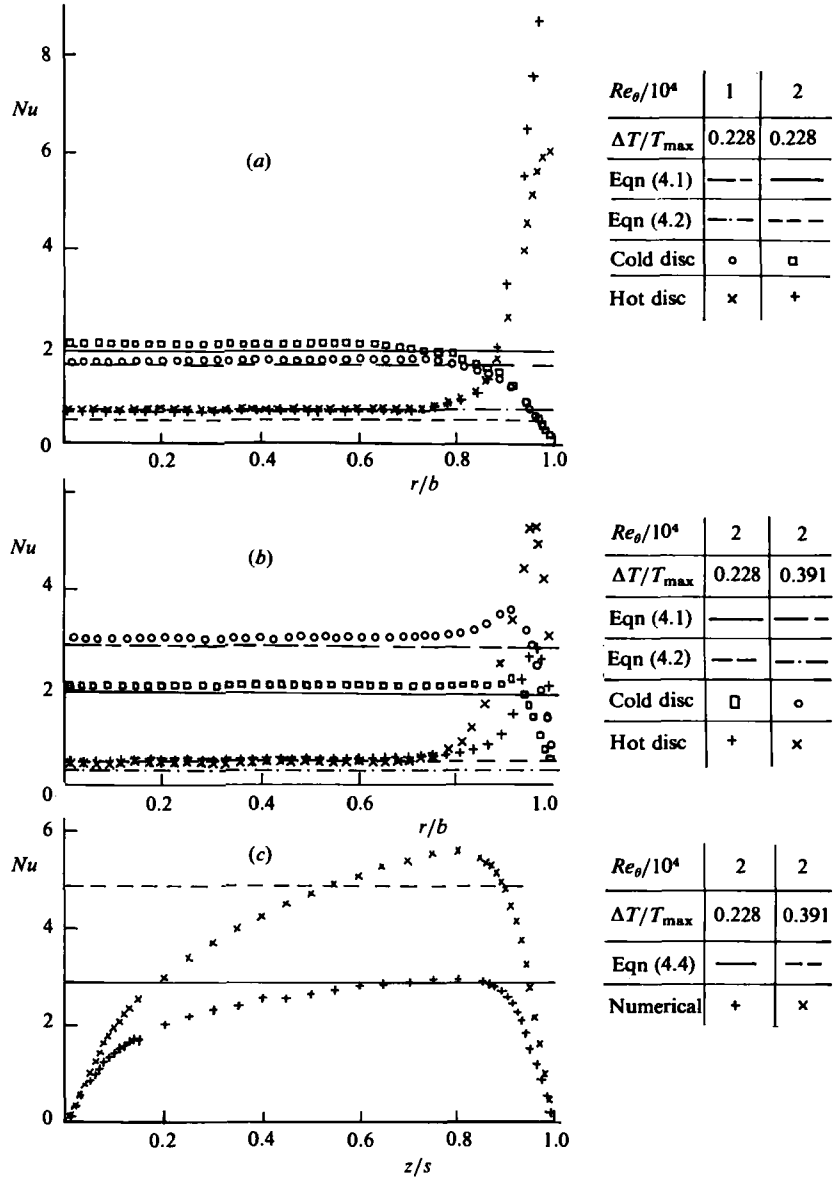

FIGURE 10. Local Nusselt numbers for an air-filled cavity with isothermal disks: (*a*) Nusselt number distribution on the disks when $\delta T/\delta r = 0$ at $r = b$; (*b*) Nusselt number distribution on the disks when $T = T_0 + (z/s)\Delta T$ at $r = b$; (*c*) Nusselt number distribution on the surface $r = b$ when $T = T_0 + (z/s)\Delta T$ at $r = b$.

cases (v) and (vi), respectively. Similarly, neglect of radial heat conduction requires that

$$\max\left\{\left|\frac{r\Delta T}{2s^2}\left(\frac{\mathrm{d}\Delta T}{\mathrm{d}r}\right)^{-1}\right|, \left|\frac{Re_\delta^{\frac{1}{2}} Pr\,\beta\,\Delta T r}{16s}\left[\frac{r}{b}+\frac{2\Delta T}{b}\left(\frac{\mathrm{d}\Delta T}{\mathrm{d}r}\right)^{-1}\right]\right|\right\}$$

is large. At r/b this parameter takes the values of 0.9 and 3.4 for cases (v) and (vi), respectively.

Local Nusselt number distributions on the disks for the results of the isothermal-

disk tests are shown in figures 10(*a*) and (*b*). For comparison with the numerical results, predictions from the similarity solutions are also shown. For the conditions considered here these are given by

$$Nu_0 = \frac{\Phi}{1-e^{-\Phi}}, \tag{4.1}$$

$$Nu_s = -\left[\frac{Pr\,\beta\,\Delta T}{8} Re_\theta^{\frac{1}{2}} \frac{sr}{b} \frac{dT_s}{dr} + \frac{\Phi}{1-e^{\Phi}}\right] \frac{k_s}{k_{ref}}, \tag{4.2}$$

where

$$\Phi = \frac{Pr\,\beta\,Re_\theta^{\frac{1}{2}}}{8r} \frac{s}{b} \frac{d(r^2\,\Delta T)}{dr}. \tag{4.3}$$

Note that the factor k_s/k_{ref} (where $k_s = k$ at temperature T_s) has been included in (4.2) to make some allowance for the increased conductivity near the hot disk: in deriving the similarity solution k was assumed constant. As before, β has been set to $1/T_{max}$. Away from the outer layer the results for all the conditions studied are in reasonable agreement with the infinite-disk theory. From the results with an adiabatic condition at $r = b$, shown in figure 10(*a*), it can be seen that the Nusselt number distributions shows qualitative similarities to the predictions for the oil-filled cavities. The main heat transfer from the hot disk occurs in the outer-layer region where cold fluid impinges on this surface while heat transfer to the cold disk is strongest towards the centre of the cavity and falls towards zero in the outer layer. As expected from the isotherm plots, a change in the thermal boundary condition at $r = b$, to a linear temperature variation, has an important effect on the heat transfer in the outer part of the cavity. Comparing the results in figures 10(*a*) and (*b*) shows that the influence of the rechannelling of fluid in the outer layer is less for the linear temperature condition, with the extent of the region in which the results depart from the similarity solution being reduced and the maximum value of the Nusselt number being lower in this case. The peak in the Nusselt number distributions on the cold disk at r/b in figure 10(*b*) is thought to be caused by the secondary recirculation at the edge of the outer layer.

Figure 10(*c*) shows the variation of the Nusselt number, defined as $Nu = sk_{ref}\,q/\Delta T$, on the cylindrical surface for the two cases in which a linear temperature distribution was assumed on this surface. Since the net mass flow of fluid across the cavity in the outer layer must equal the flow in the Ekman layers feeding into this region, an estimate of this flow rate can be obtained by calculating the mass flow in the Ekman layers at $r = b$ from the infinite-disk solution. Assuming that as the fluid flows across the cavity its mean temperature changes with axial distance z at the same rate as the cylindrical surface temperature, the Nusselt number for heat transfer from this surface can then be estimated from a simple heat balance. For a linear temperature variation this method gives the result

$$Nu = \tfrac{1}{8} Pr\,\beta\,\Delta T\,Re_\theta^{\frac{1}{2}}. \tag{4.4}$$

This relation is plotted in figure 10(*c*) for comparison with the numerical results. For case (iii) ($Re_\theta = 2\times10^4$, $\Delta T/T_{max} = 0.228$), the numerical predictions are close to these results in the region $0.6 < z/s < 0.85$, but the results over the rest of the surface, which appear to be influenced by the end conditions at $z = 0$ and s, are lower than this. The flow induced in the cavity for the other case (iv), ($Re_\theta = 2\times10^4$, $\Delta T/T_{max} = 0.391$), is somewhat stronger, and for the gap width used here the Nusselt number does not appear to reach a steady value.

The Nusselt number distributions for the two non-uniform temperature distri-

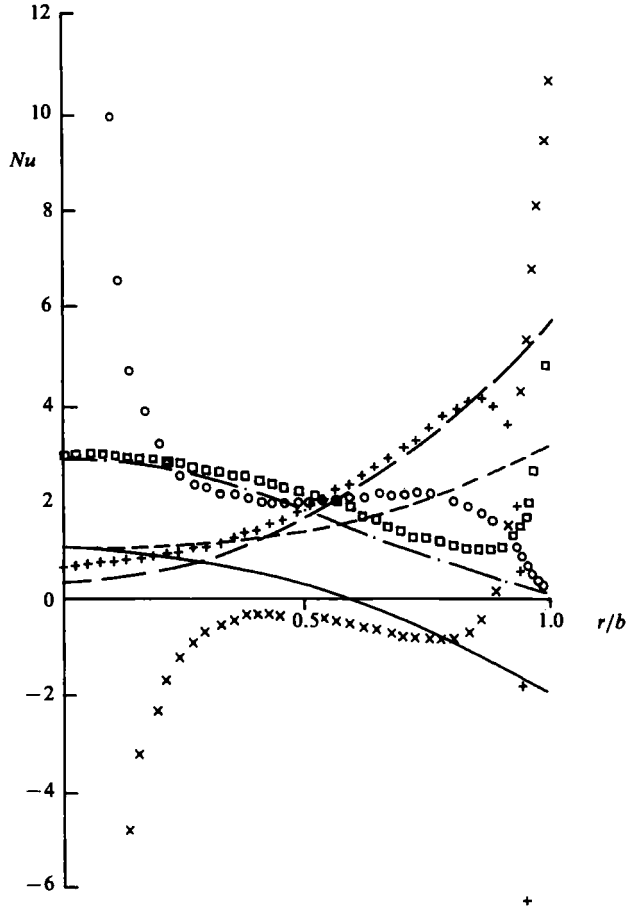

FIGURE 11. Local Nusselt numbers for an air-filled cavity with a non-uniform disk temperature.

$Re_\theta/10^4$	2	2
$\Delta T/T_{max}$	$0.228(r/b)^2$	$0.391[1-(r/b)^2]$
Equation (4.1)	– – – –	–·–·–
Equation (4.2)	——	— —
Cold disk (numerical)	○	□
Hot disk (numerical)	×	+

butions studied are shown in figure 11. Looking first at case (v), ($Re_\theta = 2 \times 10^4$, $\Delta T/T_{max} = 0.228(r/b)^2$), it is apparent that, as expected from the earlier results, the numerical and analytical solutions do not agree. The analysis of the radial outflow between co-rotating disks with $T_0 = T_s$ (Chew 1982) gives a first-order correction for radial heat conduction in the core to the Nusselt number of $2(s/r)^2$ for a quadratic temperature distribution. Although the presence of the axial wind in these buoyancy-driven flows can be expected to reduce this effect, this does give some indication of the significance of the radial conduction terms. In fact the difference between the analytical and numerical predictions is consistent with this result and the two solutions do show signs of converging as r/b increases to about 0.8, but at higher values of r/b than this the numerical results are affected by the outer layer. Numerical and analytical results for case (vi), $Re_\theta = 2 \times 10^4$, $\Delta T/T_{max} = 0.391[1-(r/b)^2]$, are in reasonable agreement for $r/b < 0.85$. The difference in the results at radii greater than this is also attributed to radial heat condition.

Mean Nusselt numbers for the different conditions studied are given in table 2. The similarity solution results, shown for comparison, were obtained by integration of the local heat fluxes given by (4.1) and (4.2). For the two cases in which ΔT varies with radius the integrals were calculated numerically. As with Hudson *et al.*'s measurements for the low-viscosity oil, the numerical results for heat transfer across a cavity with isothermal disks and an adiabatic cylindrical surface are slightly less than the similarity-solution predictions for the cold disk.

The effect of introducing a linear temperature condition on the bounding cylindrical surface is to bring the heat transfer on both disks closer to the infinite-disk theory. For the case $\Delta T/T_{\max} = 0.228(r/b)^2$ most of the heat transfer occurs in the outer part of the cavity where the effects of the cylindrical surface are most important. Considering also that radial conduction is important towards the centre of the cavity, it is not surprising that the Nusselt number for the closed cavity does not agree with the infinite-disk theory for these conditions. The numerical results for the case $\Delta T/T_{\max} = 0.391[1-(r/b)^2]$ fall midway between the analytical solutions for the hot and cold disks. The difference between the analytical results for the two disks is caused by the factor k_s/k_{ref} in (4.2). If the thermal conductivity was constant these two results would agree exactly.

5. A cavity with a radial outflow of air

Numerical results are given here for radial outflow with a uniform radial source and sink, both rotating at the same speed as the disk. The disk radius $b = 190$ mm, the inlet radius $a = 19$ mm and the axial distance between the disks $s = 50.7$ mm. A non-dimensional mass-flow parameter C_w ($= m/\mu b$, where m is the net radial mass flow rate) is introduced to characterize the radial flow rate. For the results given here, a rotational speed corresponding to $Re_\theta = 2.5 \times 10^4$ was used and two different mass-flow rates were considered, giving $C_w = 38.5$ or 79.

The boundary conditions at the source and sink were specified as follows:

$$\left.\begin{aligned} u &= \frac{Q}{2\pi as}, \quad v_\phi = \Omega a, \quad w = 0, \quad T = T_I \quad \text{at } r = a, \\ u &= \frac{Q}{2\pi bs}, \quad v_\phi = \Omega b, \quad w = 0, \quad \frac{\partial T}{\partial r} = 0 \quad \text{at } r = b. \end{aligned}\right\} \tag{5.1}$$

Here Q is the volume flow rate of air, which, owing to density variations, will be different at the inlet and outlet. The inlet temperature, T_I, was set at 288 K throughout. The velocity conditions on the two disks were unchanged from those in the previous sections. Various disk temperature distributions were specified; for $C_w = 38.5$, only one case, $T_s = T_I$, $\Delta T/T_{\max} = -0.449(r/b)^2$ was studied; for $C_w = 79$, the three cases $\Delta T/T_{\max} = -0.319(r/b)^2$, $\Delta T/T_{\max} = -0.391(r/b)^2$ and $\Delta T/T_{\max} = -0.449(r/b)^2$ with $T_s = T_I$ and the symmetric case $\Delta T = 0$, $(T_s - T_I)/T_{\max} = 0.227(r/b)^2$ were considered.

The effects of buoyancy on the flow in this case are illustrated by the streamlines for $C_w = 38.5$, $\Delta T/T_{\max} = -0.449(r/b)^2$ shown in figure 12(*a*). Towards the centre of the cavity, where buoyancy forces are less important, the flow is symmetric about the mid-axial plane. At higher radii the flow in the Ekman layer on the cold disk is increased, while that on the hot disk is reduced, with an axial flow occurring across the central core. Above a critical radius the flow on the hot disk reverses and radial inflow occurs in this Ekman layer, as for buoyancy-driven flow in a sealed cavity.

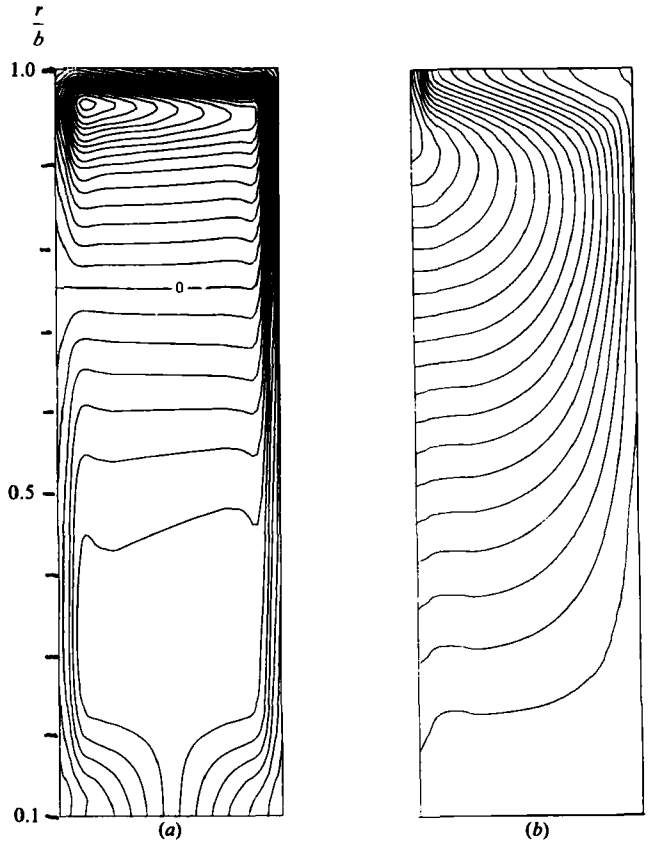

FIGURE 12. Radial outflow of air, $Re_\theta = 2.5 \times 10^4$, $C_w = 38.5$, $T_s = T_1$, $\Delta T/T_{max} = -0.449(r/b)^2$: (*a*) streamlines at intervals of 1.3×10^{-6} m^3/s, (*b*) isotherms at intervals of 10 K.

From the similarity solution it follows that the flow reversal occurs at a critical radius given by

$$\left(\frac{r}{b}\right)^2 = \frac{2C_w}{\pi Re_\theta^{\frac{1}{2}} |\beta \Delta T|}. \tag{5.2}$$

Putting $\beta = 1/T_0$ in this expression gives a value of r/b for which reversal occurs of 0.72 in this case. The numerical predictions for the other conditions studied were also in reasonable agreement with (5.2) although, as the critical radius approaches the cavity radius, the flow reversal occurs at a slightly lower radius than is predicted by this equation.

The trends shown in the streamline plots are reflected in the isotherms which are shown in figure 12 (*b*). At small radii there is a small axial temperature difference across the heated Ekman layer which decreases as the radius increases. At higher radii, but away from the influence of the rechannelling of fluid by the outer cylinder, the isotherm plots show that the temperature at the hot disk is propagated into the central core by the axial wind. The fluid temperature is then reduced to that of the cold disk as it traverses a thermal boundary layer, which is somewhat thicker than the Ekman layers.

Figure 13 shows radial and tangential velocity across the cavity for the

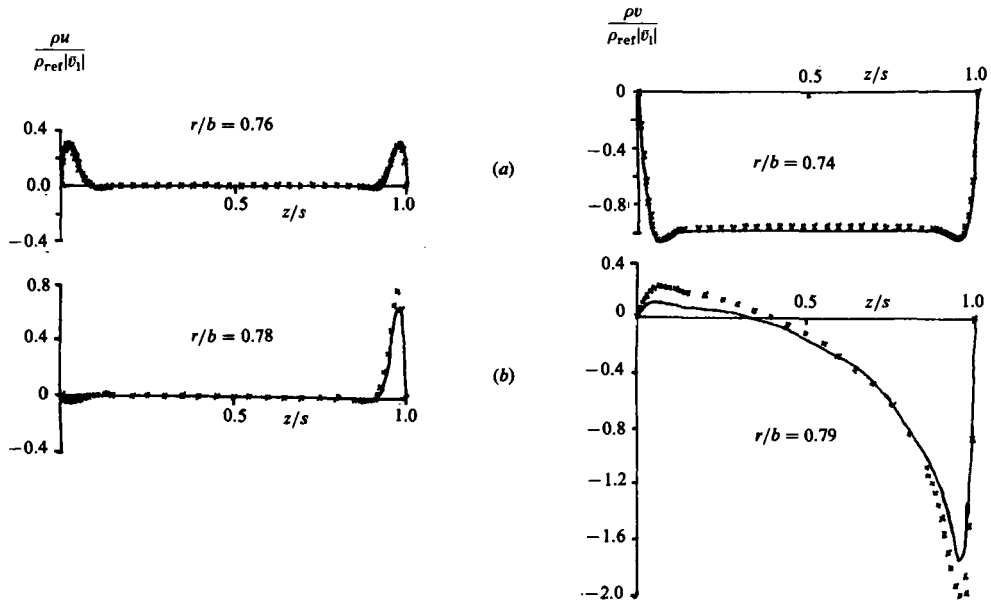

FIGURE 13. Radial and tangential velocity profiles for radial outflow of air, $Re_\theta = 2.5 \times 10^4$; (*a*) $C_w = 79$, $\Delta T = 0$, $(T_s - T_I)/T_{max} = 0.227(r/b)^2$; (*b*) $C_w = 38.5$, $\Delta T = -0.449(r/b)^2$, $T_s = T_I$; ×, numerical results; ——, similarity solution.

cases $C_w = 79$ with $\Delta T = 0$, $(T_s - T_I)/T_{max} = 0.227(r/b)^2$ and $C_w = 38.5$ with $\Delta T/T_{max} = -0.449(r/b)^2$, $T_s = T_I$. Here the velocities are normalized by division by $\bar{v}_1$, the linear isothermal prediction for the tangential velocity in the core region, which is given by

$$\bar{v}_1 = 2\epsilon_r \Omega r, \tag{5.3}$$

where ϵ_r ($= b^2 C_w / Re_\theta^{\frac{1}{2}} 4\pi r^2$) is a Rossby number for the forced flow. As before, β has been taken as $1/T_{max}$ in obtaining the results from the similarity solutions which are also shown on this figure. Considering the property variations within the fluid and the simplifying assumptions used in deriving the analytical solutions, the agreement between numerical and the theoretical results is reasonable. Comparison with the earlier results for isothermal flow suggests that, in the symmetrically heated case, the increased temperature at larger radii leads to a slight reduction in the value of $|\rho\bar{v}|$ in the outer part of the cavity.

Local Nusselt numbers, based on hot-disk-to-inlet temperature difference $(T_0 - T_I)$ for the various conditions studied, are shown in figure 14. Also shown are the results from the similarity solution which for these conditions are given by

$$Nu_s = \frac{sq_s}{k_{ref}(T_0 - T_I)} = \frac{\Phi}{1 - e^{-\Phi}}, \tag{5.4}$$

$$Nu_0 = \frac{sq_0}{k_{ref}(T_0 - T_I)} = \frac{Pr\, s}{2b}\left[\frac{C_w}{\pi}\left(\frac{b}{r}\right)^2 - \beta\frac{\Delta T}{2} Re_\theta^{\frac{1}{2}}\right] - \frac{\Phi}{1 - e^{\Phi}}, \tag{5.5}$$

where

$$\Phi = -\frac{Pr\,\beta\,\Delta T\, Re_\theta^{\frac{1}{2}} s}{2b} \tag{5.6}$$

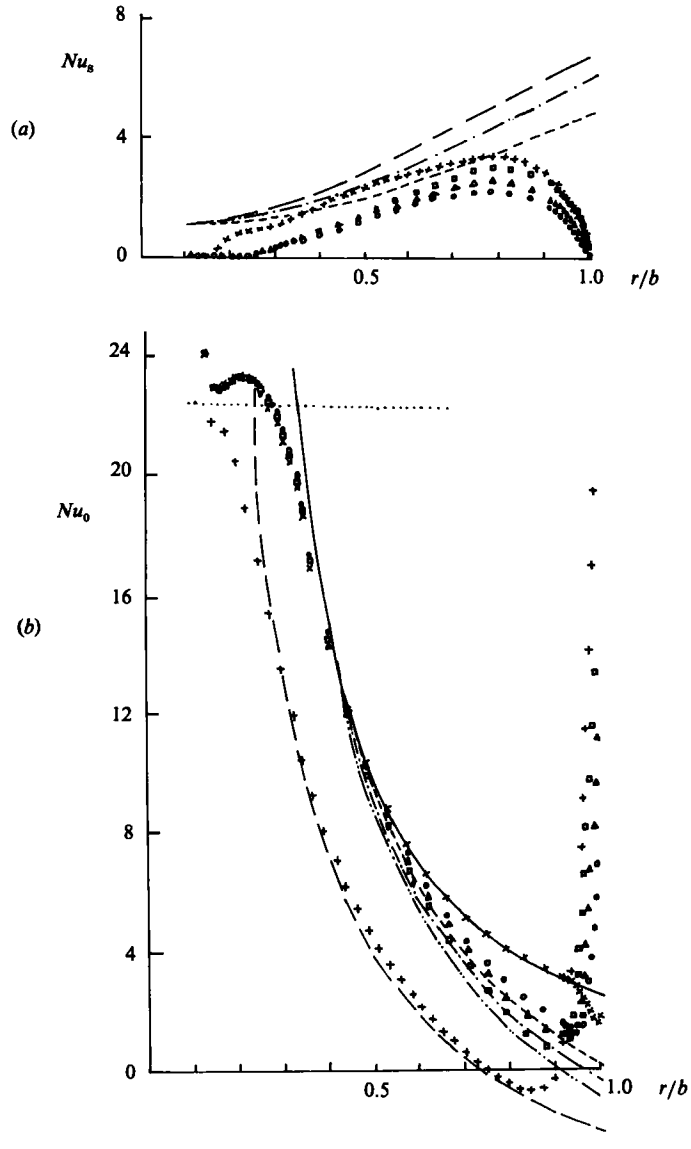

FIGURE 14. Local Nusselt numbers for radial outflow of air, $Re_\theta = 2.5 \times 10^4$, (*a*) disk $z = s$, (*b*) disk $z = 0$.

	C_w	$-\Delta T/T_{max}$	$(T_s - T_1)/T_{max}$	Numerical	Equation (5.4)	Equation (5.5)	Equation (5.7)
(i)	79	0	$0.227(r/b)^2$	×		——	·····
(ii)	79	$0.319(r/b)^2$	0	○	- - - -	- - - -	·····
(iii)	79	$0.391(r/b)^2$	0	△	-·-·-	-·-·-	·····
(iv)	79	$0.449(r/b)^2$	0	□	——	-··-··-	·····
(v)	38.5	$0.449(r/b)^2$	0	+	——	——	·····

and q_0 and q_s are the heat fluxes at the disk surfaces. Dorfman's (1963) 'free disk' result for heat transfer from the hot disk is expected to approximate the results in the 'source region' and so this is given in figure 14(*b*). For air, with a quadratic temperature distribution on the disk, this may be written

$$Nu_0 = 0.530\, Re_\phi^{\frac{1}{2}} \frac{s}{b}. \tag{5.7}$$

Note that the coefficient of thermal expansion β has been taken as $1/T_0$ here, rather than $1/T_{\max}$ as used in calculating the velocity solutions in figure 13.

Looking first at figure 13(*b*), it is apparent that buoyancy effects can lead to a reduction in heat transfer from the hot disk. As expected from earlier studies, the results for case (i), in which the two disks have identical temperature distributions, are close to (5.7) in the inner layer and (5.5) in the Ekman-layer region. In cases (ii)–(iv) the heat transfer in the Ekman-layer region is reduced as the temperature difference across the cavity increases: (5.5) appears to give a reasonable estimate of the Nusselt number in the Ekman-layer region, although the agreement for the buoyancy-affected cases, (ii)–(v), is not as good as that for case (i). As the agreement between (5.5) and the numerical result is better at the lower flow rate (case (v)) than in (ii)–(iv) it seems likely that the discrepancy between the two sets of results is caused by the neglect of nonlinear terms in the similarity solution.

The level of heat transfer to the colder disk, shown by the Nusselt number distributions in figure 14(*a*), is somewhat less than that from the hot disk. There is also a greater difference between the numerical results and the analytical solutions in this case. The influence of the outer layer appears to extend well into the cavity, reducing the heat transfer below that which would be attained between infinite disks.

6. Conclusions

A computer program previously used to study isothermal flow has been further developed to allow for buoyancy effects. In a study of centrifugally driven convection in a sealed rotating cavity two different fluids were considered: the high-viscosity silicone oil used in Hudson *et al.*'s (1978) experiments, and air. Numerical results are also presented for buoyancy-affected flow in a rotating cavity with a radial outflow of air.

Predictions of the mean Nusselt number for the high-viscosity oil ($\nu = 3.5 \times 10^{-4}$ m^2/s, $Pr = 3118$) are in good agreement with Hudson *et al.*'s measurements. In conduction-dominated conditions the numerical results for the temperature and velocity away from the outer layer are in good agreement with Dorfman's (1968) similarity solution. As convective heat transfer becomes more important the results depart from this solution and the presence of the outer cylindrical surface appears to affect the heat transfer throughout the cavity. The local Nusselt numbers are strongly dependent on radial position.

In the study of an air-filled sealed cavity attention was concentrated on the effects of the thermal boundary condition at $r = b$ and a non-uniform disk-temperature distribution. Away from the outer layer a similarity solution, which assumes constant viscosity and conductivity and uses the Bousinesq approximation for the density, still gives a reasonable representation of the flow and temperature fields despite considerable property variations. However, depending on the radial temperature distribution and the strength of the convective flow, radial viscous and heat-conduction effects, which are not taken into account in the similarity solution, may be important.

The influence of the cylindrical surface on the heat transfer to the disks is significantly reduced by the replacement of an adiabatic condition on this surface with a specified linear temperature distribution. Numerical results for the air-filled cavity with isothermal disks show that the mean Nusselt number for the cold disk falls slightly below that predicted from infinite-disk theory. The mean Nusselt number for the hot disk is strongly dependent on the thermal boundary condition on the cylindrical surface.

In radial outflow the flow may be strongly affected by buoyancy if there is an axial temperature difference between the disks. For the quadratic temperature distribution considered, the first effects of buoyancy are a reduction in the mass flow in the Ekman layer on the hot disk and a corresponding increase in the flow next to the cooler disk. This leads to a decrease in the heat transfer from the hot disk and some heat flow across the cavity to the cold disk. As buoyancy effects become dominant, the flow becomes similar to that in a sealed cavity, with the flow next to the hot disk being radially inwards. These results are also consistent with similarity solutions for the flow between two infinite disks.

This work was undertaken during the tenure of a Research Fellowship, supported by Rolls-Royce limited, at the Thermo-Fluid Mechanics Research Centre, University of Sussex. I would like to thank Dr J. M. Owen for his interest in this project.

REFERENCES

Barcilon, V. & Pedlosky, J. 1967 On the steady motions produced by a stable stratification in a rapidly rotating fluid. *J. Fluid Mech.* **29**, 673.

Chew, J. W. 1982 Computation of flow and heat transfer in rotating cavities. D. Phil. thesis, School of Engng and Applied Sciences, University of Sussex.

Chew, J. W. 1984 Development of a computer program for the prediction of flow in a rotating cavity. *Int. J. Num. Methods Fluids* **4**, 667.

Chew, J. W., Owen, J. M. & Pincombe, J. R. 1984 Numerical predictions for laminar source–sink flow in a rotating cylindrical cavity. *J. Fluid Mech.* **143**, 451.

Conlisk, A. T., Foster, M. R. & Walker, J. D. A. 1982 Fluid dynamics and mass transfer in a gas centrifuge. *J. Fluid Mech.* **125**, 283.

Dorfman, L. A. 1963 *Hydrodynamic Resistance and Heat Loss of Rotating Solids.* Edinburgh: Oliver and Boyd.

Dorfman, L. A. 1967 Laminar thermal convection in the rotating cavity between two discs. *Isv. Akad. Nauk S.S.S.R. Mech. Zhid. i Gaza* **3**, 40.

Gosman, A. D. & Ideriah, F. J. K. 1976 TEACH-T: A general computer program for two-dimensional, turbulent recirculating flow. *Dept. of Mech. Engng Report, Imperial College, London.*

Homsy, G. M. & Hudson, J. L. 1969 Centrifugally driven thermal convection in a rotating cylinder. *J. Fluid Mech.* **35**, 33.

Hudson, J. L. 1968 Non-isothermal flow between rotating discs. *Chem. Engng Sci.* **23**, 1007.

Hudson, J. L., Tang, O. & Abell, S. 1978 Experiments on centrifugally driven thermal convection in a rotating cylinder. *J. Fluid Mech.* **86**, 147.

Matsuda, T. & Hashimoto, K. 1976 Thermally, mechanically or externally driven flows in a gas centrifuge with insulated horizontal end plates. *J. Fluid Mech.* **78**, 337.

Patankar, S. V. & Spalding, D. B. 1972 A calculation procedure for heat, mass and momentum transfer in three-dimensional parabolic flow. *Intl J. Heat Mass Transfer* **15**, 1787.

Williams, G. P. 1967 Thermal convection in a rotating fluid annulus: Part 1. The basic axisymmetric flow. *J. Atmos. Sci.* **24**, 144.